

The Alpine snow-albedo feedback in regional climate models

Journal Article**Author(s):**

Winter, Kevin J. -P.M.; Kotlarski, Sven; Scherrer, Simon C.; Schär, Christoph

Publication date:

2017-02

Permanent link:

<https://doi.org/10.3929/ethz-b-000116155>

Rights / license:

[In Copyright - Non-Commercial Use Permitted](#)

Originally published in:

Climate Dynamics 48(3), <https://doi.org/10.1007/s00382-016-3130-7>

Funding acknowledgement:

136279 - The evolution of mountain permafrost in Switzerland (SNF)

The Alpine snow-albedo feedback in regional climate models

Kevin J. -P. M. Winter¹ · Sven Kotlarski^{1,2} · Simon C. Scherrer² · Christoph Schär¹

Received: 30 July 2015 / Accepted: 13 April 2016 / Published online: 29 April 2016
© Springer-Verlag Berlin Heidelberg 2016

Abstract The effect of the snow-albedo feedback (SAF) on 2m temperatures and their future changes in the European Alps is investigated in the ENSEMBLES regional climate models (RCMs) with a focus on the spring season. A total of 14 re-analysis-driven RCM experiments covering the period 1961–2000 and 10 GCM-driven transient climate change projections for 1950–2099 are analysed. A positive springtime SAF is found in all RCMs, but the range of the diagnosed SAF is large. Results are compared against an observation-based SAF estimate. For some RCMs, values very close to this estimate are found; other models show a considerable overestimation of the SAF. Net shortwave radiation has the largest influence of all components of the energy balance on the diagnosed SAF and can partly explain its spatial variability. Model deficiencies in reproducing 2m temperatures above snow and ice and associated cold temperature biases at high elevations seem to contribute to a SAF overestimation in several RCMs. The diagnosed SAF in the observational period strongly influences the estimated SAF contribution to twenty first century temperature changes in the European Alps. This contribution is subject to a clear elevation dependency that is governed by the elevation-dependent change in the number of snow days. Elevations of maximum SAF contribution range from 1500 to 2000 m in spring and are found above 2000 m in summer. Here, a SAF contribution to the total simulated temperature change between 0 and 0.5 °C until

2099 (multi-model mean in spring: 0.26 °C) or 0 and 14 % (multi-model mean in spring: 8 %) is obtained for models showing a realistic SAF. These numbers represent a well-funded but only approximate estimate of the SAF contribution to future warming, and a remaining contribution of model-specific SAF misrepresentations cannot be ruled out.

Keywords Snow-albedo feedback · European Alps · Regional climate models · ENSEMBLES · Climate change

1 Introduction

Snow cover is an important element of the climate system. The presence of snow modulates surface properties, such as the albedo, the surface radiation budget and the turbulent surface-atmosphere fluxes (Peixoto and Oort 1992). Its occurrence is governed by topography and the prevailing climatic conditions and, hence, is strongly affected by climatic changes. The latest IPCC report (2013) indicates a significant decrease of annual snow cover extent in the Northern Hemisphere over the second half of the twentieth century (Vaughan et al. 2013). For the period 1979–2012, the decrease ranges from 2.2 % per decade in March and April to 14.8 % per decade in June. In the Swiss Alps the mean snow depth and the continuous snow cover duration at low elevations decreased significantly since the 1980s (Scherrer et al. 2004, 2013; Laternser and Schneebeli 2003; Marty 2008). The documented snow cover decrease, globally and locally, correlates negatively with the temperature increase over the last decades (Vaughan et al. 2013; Scherrer et al. 2004). Note that we here define snow cover as the presence of snow both in the spatial and the temporal dimension.

✉ Sven Kotlarski
sven.kotlarski@meteoswiss.ch

¹ Institute for Atmospheric and Climate Science ETH, Zurich, Switzerland

² Federal Office of Meteorology and Climatology MeteoSwiss, Zurich-Airport, Switzerland

Due to the high albedo of snow-covered surfaces and the gradual decrease of the snow albedo with time, an accelerated metamorphism and melting of snow as a consequence of higher temperatures ultimately lead to a reduction of surface albedo (Barry and Chorley 2010). As a result, more solar radiation is absorbed by the ground, eventually leading to a further increase of near-surface air temperatures (Peixoto and Oort 1992). This positive feedback is called snow-albedo feedback (SAF); it is one of the most important feedbacks active in the climate system (Barry and Chorley 2010; Scherrer et al. 2012). The importance of the SAF can be illustrated by the fact that over the extratropics the largest warming in the second half of the twentieth century occurred at the annual-mean zero-degree isotherm (Pepin and Lundquist 2008). Both the reduction of snow cover extent and accelerated snow metamorphism contribute to the SAF. In the Northern Hemisphere the snow cover reduction is the driving component of the SAF (Fernandes et al. 2009; Qu and Hall 2007). Even though the albedo difference between typical snow cover and bare soil is smaller in spring compared to autumn, the SAF is stronger in spring. This arises from the distinct seasonal cycle of snow cover and the high incoming solar radiation in spring, which induces a considerable energy surplus (Armstrong and Brun 2008; Hall 2004).

On a global scale, previous work has quantified a surface albedo feedback in global climate models (GCMs), based on the framework of the global climate sensitivity (e.g., Winton 2006). These analyses have been carried out using multiple GCMs resulting in a mean SAF estimate between 0.26 and 0.4 $\text{W m}^{-2} \text{K}^{-1}$ (Soden and Held 2006; Colman 2003; Winton 2006). Graverson et al. (2014) recently quantified the feedback to 0.6 $\text{W m}^{-2} \text{K}^{-1}$. This high value may derive from interactions with other feedbacks, such as the lapse-rate feedback.

The current study is concerned with quantifying the regional SAF over the European Alps based on regional climate model (RCM) experiments. For this purpose, a different approach to quantify the SAF is applied, and the SAF is defined based on local 2m temperature effects following Scherrer et al. (2012, further on referred to as S2012). The latter quantify the SAF in the Swiss Alps using surface temperature and snow cover observations from nearby station pairs. The methodology yields an estimate of the effect of snow removal on ambient daily mean 2m temperature. A mean 2m temperature increase of 0.4 °C in springtime was found. This estimate was based on six station pairs in Switzerland that showed similar SAF estimates ranging from 0.3 to 0.5 °C and no clear dependence on station location or the elevation range covered by the respective station pair was apparent. The derived mean value of 0.4 °C can therefore be considered as a robust estimate valid for a larger region. Based on this estimate S2012 derived a contribution

of the SAF to the total Alpine warming trend in April in the period 1961–2011 of 3 to 7 %.

As the presence of snow, and consequently the associated long-term changes, considerably depend on elevation, the SAF and its corresponding temperature effects can be assumed to be elevation-dependent as well (e.g., Pepin et al. 2015). Investigations in the Swiss Alps suggest that this effect is rather small and the influence of large-scale flow variability on the elevation profile of temperature trends might often be larger. While Appenzeller et al. (2008) only found a clear elevation dependence in autumn using station observations in the 1961–2005 period, Ceppi et al. (2012) were able to reveal relatively small elevation-dependent warming trends also in spring using a gridded Swiss temperature data set for the 1959–2008 period. They showed that in autumn the strongest trends occur in low-lying regions (<800 m), whereas in spring the strongest warming occurs at higher reaches (≥ 1500 m). The SAF could contribute to this elevation-dependent trend, especially in spring when the strongest temperature trends approximately coincide with the elevation of the zero-degree and the snow line (Ceppi et al. 2012; Pepin and Lundquist 2008; S2012) and when the influence of larger-scale flow variability on the elevation profile of temperature trends appears to be negligible. An elevation dependence of temperature trends is also visible in global and regional climate model simulations, with a distinct warming at medium to high elevations above about 1500 m, which can at least partly be attributed to the SAF (Bradley et al. 2004; Giorgi et al. 1997; Kotlarski et al. 2012, 2015).

GCM and RCM scenarios of the twenty first century climate indicate a further reduction in snow cover extent and a shorter snow season, with later first snow in autumn and earlier melt out in spring (Collins et al. 2013; Räisänen and Eklund 2012; Lawrence and Slater 2010; Steger et al. 2013). The SAF can therefore be expected to further contribute to twenty first century temperature changes, depending on the magnitude of the SAF and the extent of snow cover reductions. A quantification of this contribution, particularly on regional scales, is currently missing.

To partly fill this gap, the aim of the present study is to validate and quantify the SAF in RCM experiments over the Alpine region based on the methodological framework of S2012. We explicitly focus on the spring season (MAM: March, April, May) during which Alpine SAF effects can be expected to be largest and most robust owing to (a) larger incoming solar radiation amounts compared to winter, (b) pronounced snow cover changes both in past records (e.g., S2012) and in future snow cover scenarios (Steger et al. 2013), and (c) a negligible influence of large-scale flow variability on historical temperature trend profiles (S2012). However, as high-elevation snow cover changes are also found for early summer

and incident solar radiation amounts are largest then, we partly also include the summer season (JJA: June, July, August) in our assessment. Both re-analysis-driven (1961–2000) and GCM-driven experiments (1951–2009) are considered. The latter are also used to quantify the contribution of the SAF to twenty first century Alpine temperature changes. In particular, the following research questions are addressed:

1. What is the magnitude of the SAF in state-of-the-art RCMs in the Alpine region, and how does it compare to observational estimates?
2. What are the physical drivers of and the processes behind the simulated SAF?
3. How are RCM temperature biases connected to the SAF?
4. What is the estimated contribution of the SAF to future Alpine temperature changes?

The following section provides information about the RCM data and the applied methods. The validation of the springtime SAF in re-analysis-driven RCM simulations and the contribution of the SAF to future temperature changes are presented in Sects. 3 and 4. The study ends with Sect. 5 that gives a concluding summary and an outlook on further aspects worth considering.

2 Data and methods

2.1 RCM data

The RCM data used in this study has been provided by the ENSEMBLES project (van der Linden and Mitchell 2009). Both re-analysis-driven (ERA40; Uppala et al. 2005) and GCM-driven RCM experiments are available, applying multiple RCMs over a common model domain using a common spatial resolution of about 25 km. The common RCM domain covers Europe with parts of the Mediterranean Sea and Africa, whereas the focus of this research is on the Alpine sub-region and the surrounding areas (see Fig. 1). For this analysis domain, mean daily 2m temperature and daily surface snow water equivalent (SWE) were extracted from all experiments. Note that the employed RCM resolution of 25 km implies a substantial smoothing of high-resolution Alpine topographic features, which is illustrated by a comparison between Fig. 1a, b. Very high-elevations above 3000 m and several major inner-alpine valleys, for instance, are not represented by the RCMs. In total, 14 ERA40-driven RCM experiments are validated with respect to their ability to represent the springtime SAF in the period 1961–2000. Furthermore, 10 GCM-driven RCMs provide transient climate scenarios for the period

1951–2009 (see Table 1), assuming greenhouse gas concentrations according to the SRES A1B emission scenario (Nakićenović and Swart 2000) up from the year 2001. These scenario simulations are used to quantify the absolute and percentage contribution of the SAF to total temperature changes in the twenty first century. In the remainder of this article, the ERA40-driven experiments will be referred to by the naming convention INSTITUTE-RCM and the GCM-driven experiments by INSTITUTE-DRIVING GCM according to Table 1.

2.2 Snow cover parameterization in RCMs

All RCMs analysed in the present work employ simplified snow cover schemes as part of their physical parameterization packages. In many cases these schemes were inherited from land surface parameterizations of global climate models. Their primary purpose is to provide a realistic lower boundary condition for the atmospheric model components, especially for the boundary layer parameterizations, in case of snow coverage. Also soil thermal and hydrological processes strongly depend on the presence of snow cover with corresponding influences, for instance, on evapotranspiration rates. The individual RCM parameterizations differ from each other but can be classified into either simple composite/single layer schemes or intermediate-complexity schemes (e.g., Boone and Etchevers 2001). While the first class considers either composite snow-soil layers or a single explicit snow layer on top of the soil, the second class employs multiple snow layers, accounting for a larger number of snow thermal and hydrological processes.

As an example, we here briefly present the snow cover parameterization of the RCM (COSMO-)CLM (e.g., Rockel et al. 2008) for which a detailed SAF validation is carried out in Sect. 3. See also Figure ESM 1 in Steger et al. (2013) for a schematic overview on the scheme. Please note that we here refer to the regional climate model CLM (COSMO-model in CLimate Mode) employed within ENSEMBLES and not to the Community Land Model (CLM; e.g., Lawrence et al. 2011) that uses the same abbreviation. Snow cover in CLM is represented by a single snow layer that sits on top of the (multi-layer) soil column and that is nourished by snowfall and depleted by snow sublimation (evaporation from the snow reservoir) and snow melt. For thermal processes, the snow layer is treated as a separate layer with a maximum depth of 1.5 m for which the mean temperature is predicted in every time step. The snow surface temperature, i.e., the interface temperature to the atmospheric model components, is diagnosed from the soil surface temperature and the snowpack mean temperature by linear extrapolation. Snow melt occurs if the soil surface temperature or the snow surface

temperature exceed the melting point of 0 °C. An ageing effect of the snowpack is accounted for and influences both the prognostic snow density (which increases with time due to snow compaction) and the snow albedo (which decreases with time due to several metamorphism processes). For small snow water equivalents of less than 1.5 cm a fractional snow coverage is considered when calculating the grid box mean evaporation flux. For further details the reader is referred to Doms et al. (2011).

Table 1 List of analysed RCM experiments: ERA40-driven RCMs to quantify and evaluate the SAF and GCM-driven RCMs to quantify the contribution of the SAF to twenty first century temperature changes. An empty entry in the third column denotes RCMs for which only the ERA40-driven experiment has been analysed. Note that only a sub-set of GCM-driven ENSEMBLES simulations is considered (see Sect. 2.5 for details)

INSTITUTE	RCM	DRIVING GCM
C4I	RCA	–
CNRM	Aladin	–
DMI	HIRHAM	ARPEGE
EC	GEMLAM	–
ETHZ	CLM	HadCM3Q0
KNMI	RACMO	ECHAM5
METNO	HIRHAM	–
METO	HadRM3Q0	HadCM3Q0
	HadRM3Q16	HadCM3Q16
	HadRM3Q3	HadCM3Q3
MPI	REMO	ECHAM5
OURANOS	CRCM	–
SMHI	RCA	BCM ECHAM5 HadCM3Q3
UCLM	PROMES	–

Despite the use of such simplified snow schemes, previous works indicate the value of direct GCM and RCM snow cover output to assess future snow cover changes on different spatial scales and to complement the application of dedicated snow models driven by climate model output. Steger et al. (2013), for instance, validated snow amounts and snow coverage as represented by the ENSEMBLES RCMs for the European Alps (i.e., for the same set of models and the same region that are considered in the present work) and analysed the projected future changes. A decent representation of Alpine snow cover with respect to its spatial and temporal variability was found. The multi-model mean of the ERA40-driven ensemble accurately represents mean winter SWE at elevations below 1500 m which is, however, partly due to compensating biases in the individual RCMs. SWE at high elevations is typically overestimated, which can partly be attributed to large positive precipitation biases and cold temperature biases (which are also apparent for the GCM-driven climate scenario runs of ENSEMBLES; see Kotlarski et al. 2015). For the GCM-driven climate scenarios, Steger et al. (2013) also revealed snow accumulation deficiencies in individual model runs, i.e., a constantly accumulating snow cover at high elevations. Based on these previously obtained results, the respective model experiments were excluded from the scenario analysis in the present paper (see also Sect. 2.5).

2.3 SAF quantification

To quantify the SAF the methodology introduced by S2012 is applied. It consists of a comparison of 2m temperatures at two nearby stations for snow-covered and snow-free days and is illustrated in Fig. 2. In the frame of the present work, this methodology is transferred from the station scale considered by S2012 to the scale of RCM grid cells. For the final SAF assessment, the even larger Alpine-wide scale (here called *regional* scale) is considered by deriving

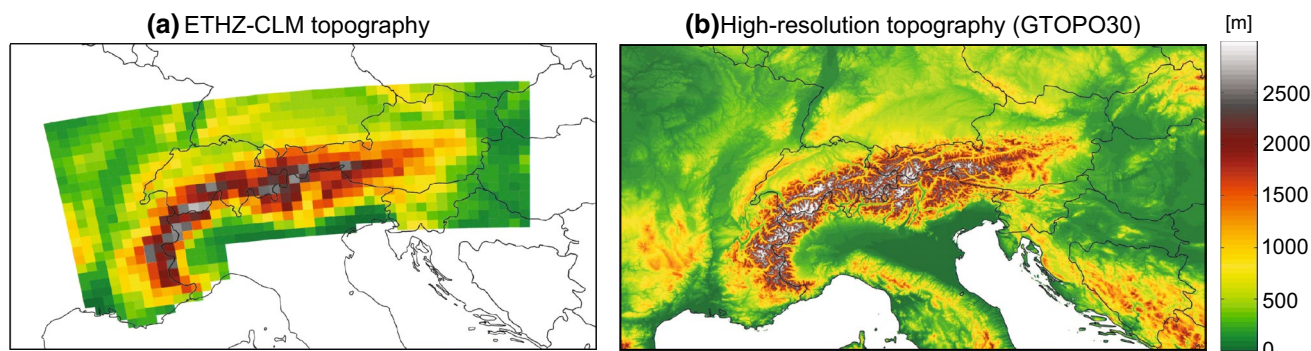
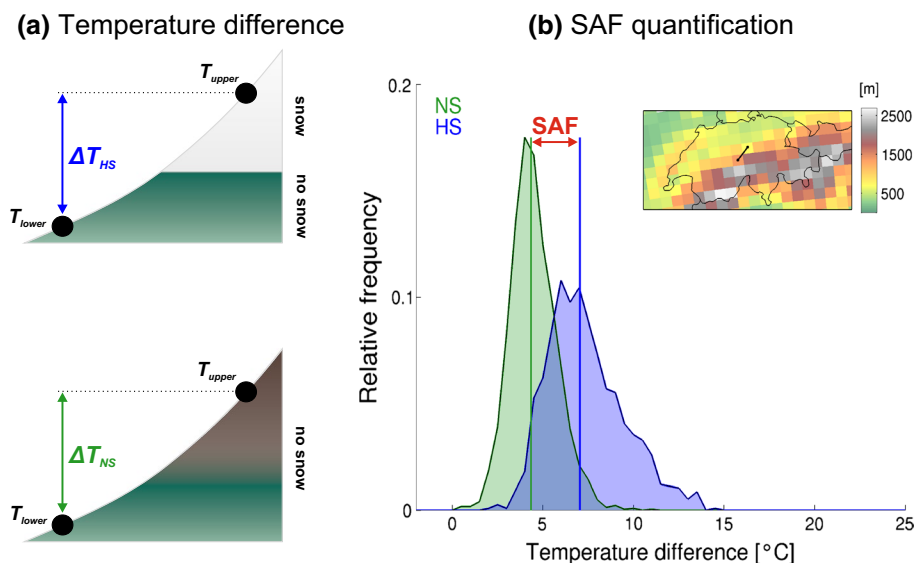


Fig. 1 **a** Illustration of the Alpine topography of the regional climate model ETHZ-CLM. The coloured area indicates the analysis domain used in the present study. **b** High resolution topography (approx-

mately 1 km) of the Alpine region as represented by the digital elevation model GTOPO30 (US Geological Survey 2014)

Fig. 2 Schematics of SAF quantification. **a** Calculation of temperature differences following S2012 in the two samples: *HS* (“high snow”, upper panel) and *NS* (“no snow”, lower panel). **b** Distribution of daily temperature differences ($T_{lower} - T_{upper}$) in spring for both samples in the period 1961–2000 for one particular grid cell pair in ERA40-driven ETHZ-CLM. The difference between the two medians (vertical lines) reveals a SAF of 2.7 °C. The map on the top right shows the geographical location of the two grid cells analysed



SAF estimates valid for the entire analysis domain. Since the RCMs do not provide snow depth data but SWE values, an SWE threshold of 0.01 m is defined at which a given grid cell is considered as snow-covered. The use of different SWE thresholds does not change the diagnosed SAF considerably (not shown). Assuming an average wind-toughened snow density of 300 kg m⁻³ (Barry and Gan 2011) our threshold corresponds to a snow depth of approx. 0.033 m.

To isolate and quantify the SAF, pairs of neighbouring RCM grid cells located at different elevations are analysed with respect to their temperature difference (lower grid cell minus upper grid cell) for days at which the upper grid cell is snow-covered and the lower one is snow-free (further referred to as *HS* for “high snow”). The same is done for days at which both grid cells are snow-free (further referred to as *NS* for “no snow”). The SAF is defined as the median difference of the two distributions:

$$SAF = \overbrace{median(T_{lower} - T_{upper})}^{HS} - \overbrace{median(T_{lower} - T_{upper})}^{NS} \quad (1)$$

with T_{lower} indicating the temperature at the lower grid cell and T_{upper} the temperature at the upper grid cell. In this scheme, the computed SAF is essentially a measure of the SAF at the upper grid cell. The analysis is carried out separately for each season under consideration.

Assuming a cooling effect of snow cover on 2m temperatures, temperature differences for *HS* can generally be expected to be larger compared to *NS*. See Fig. 2a for an illustration of the method, and Fig. 2b for an example of diagnosed *HS* (blue) and *NS* (green) temperature differences for a particular grid cell pair, a particular model (ETHZ-CLM) and a specific season (spring). The applied

method involves a sampling of specific days and specific weather situations in the two samples governed by larger-scale flow variability. These situations can be associated with, e.g., inversions and modifications of standard atmospheric temperature lapse rates and have a potential to mask any snow cover-induced temperature anomalies. As a consequence, the two probability density functions (PDFs) are not entirely distinct from each other but partly overlap. A sufficiently large number of days for both the *HS* and the *NS* sample is needed to ensure a robust diagnosis of the SAF. Therefore, a minimal number of days to be contained in each individual sample is defined. If this criterion is not met, the SAF is not calculated for this particular grid cell pair and season. In S2012 the samples consist of at least 1000 values for the 50-year period. Since our analysis period has a length of 40 years only, a minimal number of 800 values per sample is selected, which corresponds to 20 days per season (or about 7 days per month). The required minimal number of days also implies a sufficiently large elevation difference between both grid cells as grid cell pairs with similar elevations would be associated with a too small *HS* sample. For ETHZ-CLM the elevation differences range from approximately 50 to 1400 m (see Figs. 5 and 6a) and completely cover the range of elevation differences considered by S2012. Also note that the established criterion of a minimal number of days per sample is associated with different samples of grid cell pairs in the individual seasons.

Since the diagnosed SAF depends on the elevation differences in the represented samples of grid cell pairs (see Sect. 3.1.3), an elevation-normalised SAF is needed. To this end, a least-square linear regression through all diagnosed SAFs and the associated elevation differences is calculated (see later in Fig. 5) and the extrapolation of the regression

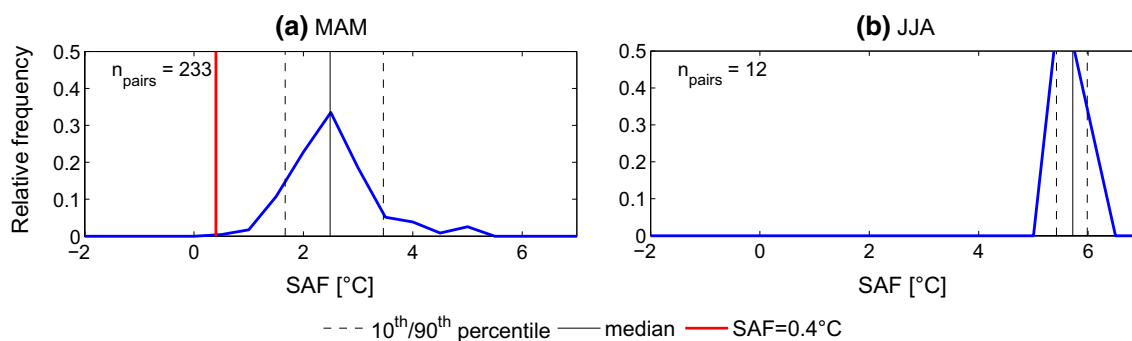


Fig. 3 PDFs of diagnosed SAF values of ETHZ-CLM in **a** MAM and **b** JJA for the period 1961–2000, using 0.5° bins. The vertical axis presents the fraction of grid cell pairs with a given SAF-value, and n_{pairs} indicates the number of grid cell pairs contributing to the particular PDF. Additionally, the median (vertical solid line), 10th and

90th percentiles (vertical dashed lines) are marked. SAF values are calculated if both the *HS* and *NS* class include at least 800 values. The SAF determined by S2012 for MAM from observations is shown as red line

line to 0 m reveals an elevation-normalised SAF (further referred to as *0m-SAF*). The *0m-SAF* is considered as the primary estimate of the regional SAF in the Alpine area in this study. As uncertainty estimate, it is complemented by the median SAF and the 10th and 90th percentiles of the spatial SAF distribution in the respective season and the respective model experiment (see Fig. 3).

2.4 Validation data

The diagnostic method for SAF quantification in the RCMs as described above is based on the methodology employed by S2012. For the spring season, the latter found a mean springtime SAF of 0.4°C based on station observations. This value serves as a reference, against which the SAF values diagnosed from the individual RCM experiments will be compared. Note that only the springtime SAF can be validated by this approach. Further seasons are not considered in the validation exercise.

2.5 SAF in climate scenarios

In the climate scenario part of this study, the contribution of the SAF to local and regional twenty first century temperature changes is quantified. For this purpose, several GCM-driven RCM experiments of the ENSEMBLES project are excluded and only those experiments are retained that (a) do extend until the year 2099, (b) do not show serious snow accumulation deficiencies (Steger et al. 2013) and (c) use a compatible calendar for daily temperature and daily SWE data (see Table 1). The contribution of the SAF to future temperature changes is quantified using the diagnosed SAF for the respective season in the ERA40-driven experiments. This is only feasible if the diagnosed SAF shows a similar magnitude in both the re-analysis-driven and the GCM-driven run of a particular model.

An analysis of the SAF in the GCM-driven ETHZ-Had-CM3Q0 experiment over the same period (1961–2000) using the same method reveals similar PDFs of SAF values as for the re-analysis-driven ETHZ-CLM run (not shown). We therefore assume that the diagnosed SAF in the ERA40-driven experiments can also be applied for the GCM-driven simulations.

After quantifying and validating the SAF in the ERA40-driven experiments, all RCMs are sorted into two categories. An acceptable range of SAF values in MAM from 0 to 1°C , based on the value of 0.4°C found by S2012 is defined. Models revealing a *0m-SAF* between 0 and 1°C in MAM are used to quantify the contribution of the SAF to temperature changes in the twenty first century and will be referred to as *SAF models*. Models that reveal an unrealistically high or low SAF have to be treated more carefully, as the diagnosed SAF probably reflects model temperature biases depending on the presence of snow cover (e.g., Buzzi 2008 for the case of ETHZ-CLM). For instance, a distinct snow cover-induced cold temperature bias can result in an overestimation of the diagnosed SAF. Such models will be discussed separately in the climate scenario analysis and are therefore referred to as *other models*. Note that the climate scenario analysis considers the JJA season in addition to MAM, but that the validation exercise on which the model selection is based has been carried out for MAM only. We therefore implicitly assume that the validation results obtained for MAM also apply to JJA.

The change in the number of snow days (ΔSD) in 2070–2099 compared to the reference period 1971–2000 is used to quantify the SAF contribution to temperature changes between these two periods. For a given model and season, the relative change in snow days ($\frac{\Delta SD}{\text{alldays}}$) multiplied by the diagnosed *0m-SAF* (*SAF*) from the ERA40-driven simulations is assumed to determine the contribution of the SAF to the total future temperature change (ΔT_{SAF}):

$$\Delta T_{SAF} = \frac{\Delta SD}{\text{all days}} \cdot SAF \quad (2)$$

An uncertainty estimate of ΔT_{SAF} is provided by using the median SAF, 10th and 90th percentiles of the spatial SAF distribution in addition to the 0m-SAF (see Sect. 2.3). Both, absolute and percentage ΔT_{SAF} values are presented. The latter are calculated by dividing ΔT_{SAF} by the total temperature change ΔT . Since snow day changes are strongly dependent on elevation (Ceppi et al. 2012), the climate scenario analysis is carried out for 500 m elevation bands. When calculating the SAF contribution as described in Eq. 2, the SAF is assumed to be stationary in time. This assumption is crucial for the results, but additional analyses for the period 2070–2099 (not shown) indicate no major change of the SAF between the reference and the scenario period for a given model.

3 SAF in re-analysis-driven RCMs

This section presents the validation of the springtime SAF in the ERA40-driven experiments over the period 1961–2000. The first part focuses on the RCM ETHZ-CLM, for which the diagnosed SAF is investigated in detail. Specific issues of the model and methodological details are discussed. In a second part all ERA40-driven RCMs of the ENSEMBLES project are considered and the SAF is quantified for the entire ensemble.

3.1 Validation in ETHZ-CLM

3.1.1 SAF quantification

In ETHZ-CLM, 3196 grid cell pairs exist in the analysis domain that can be used to diagnose the SAF. Yet, the *HS* and *NS* samples need to contain data of at least 800 days (see Sect. 2.3). This criterion reduces the number of grid cell pairs diagnosing the SAF to 233 in MAM and to only 12 in JJA. As expected, the two distributions of temperature differences are clearly separable. The PDF of the sample *HS* is distinctly shifted towards larger temperature differences compared to *NS* (e.g., Fig. 2b). The diagnosed SAF values in ETHZ-CLM are illustrated in Fig. 3 and, for springtime, vary between about 0.5 and 5.5 °C. These results indicate that simulated 2m temperatures in MAM are on average 2.49 °C (median of distribution) warmer on snow-free days than on snow days. This value is considerably larger than the one diagnosed by S2012 from observations (0.4°). This mismatch may derive from a systematic model bias in the 2m temperature diagnostics relating to difficulties of ETHZ-CLM in reproducing near-surface temperature profiles. This issue has been closely

investigated by Buzzi (2008). It is obviously connected to shortcomings of the model's boundary layer transfer scheme and a partly misrepresented effective canopy height at grid cells with a large orographic roughness length (that are particularly found in the Alpine region). As a result, erroneous near-surface temperature profiles are used and 2m temperatures in ETHZ-CLM are often too strongly coupled to the surface temperatures. In case of the presence of a snow pack (low surface temperature and stable boundary layer) this leads to an underestimation of the diagnosed 2m temperature above snow, which can be assumed to strongly affect the diagnosed SAF. This deficiency may partly explain the strong overestimation of the SAF in ETHZ-CLM, but other models could be affected by similar biases as well. It is important to note that the described problem is directly connected to the way the SAF is diagnosed in the frame of the present work. The applied scheme relies on the 2m temperature and any shortcoming in the diagnosis of this quantity will directly affect the derived SAF, in particular if the quality of the diagnosis is dependent on the presence of a snow pack. Different SAF estimation schemes, for instance those explicitly relying on the surface energy balance, would not necessarily be affected.

For both seasons a large spread of SAF values is obtained for the individual grid cell pairs. A more detailed analysis reveals that the spatial variability of the diagnosed SAF is not random and is partly connected to the elevation of the upper grid cell: high-elevation grid cells often diagnose a larger SAF compared to grid cells at low elevations (not shown). In JJA a much narrower PDF is obtained. This may result from the small number of grid cell pairs diagnosing a SAF in this particular season. The SAF spread is further discussed in the following Sect. 3.1.3. Also, the regional SAF is larger in JJA than in MAM, which is possibly connected to the seasonal cycle in global radiation with larger incoming radiation in the summer season (e.g., Cess et al. 1991; Barry and Chorley 2010).

3.1.2 Physical drivers of the SAF

To evaluate the driving processes behind the SAF and to determine their relative influence, the relation between key variables of the surface energy budget (net shortwave and longwave radiation, latent and sensible heat flux, albedo) and the diagnosed SAF for the spring season is investigated: An albedo change induced by snow cover reduction can be thought to result in increasing 2m temperatures mainly because of larger net shortwave radiation. Additionally, Ohmura (2001) shows that incoming longwave radiation provides the largest energy source influencing 2m temperatures. The sensible heat flux and the partitioning between sensible and latent heat fluxes constitute additional influences of surface energy balance parameters

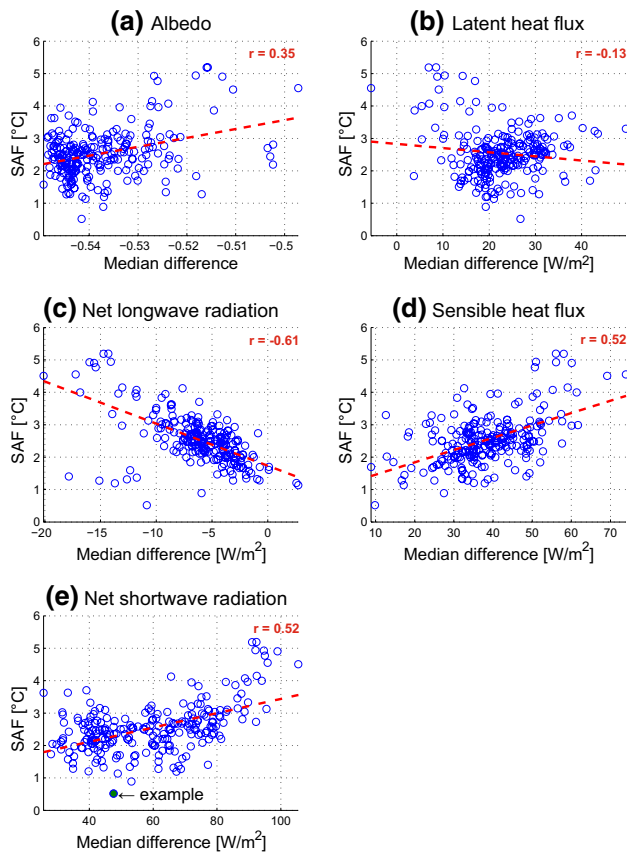


Fig. 4 Relationship between the SAF and the median difference of **a** albedo, **b** net latent heat flux, **c** net longwave radiation, **d** net sensible heat flux and **e** net shortwave radiation for MAM in ETHZ-CLM. Data points are shown for all grid cell pairs that enable the computation of the SAF. The *red line* shows a linear regression. The *filled circle* in (e) is discussed in the text

on near-surface temperature conditions. To identify the main drivers of the SAF, the same analysis that was used to diagnose the SAF (see Eq. 1) was carried out for the parameters of the surface energy balance. A median difference between *HS* and *NS* for each variable was calculated. Comparing the resulting median difference to the SAF, a positive correlation is expected since larger median differences in available surface energy can be thought to induce larger temperature differences and consequently a larger SAF. The resulting relationships between energy balance components and the SAF for MAM are presented in Fig. 4. The albedo median differences calculated according to Eq. 1 show negative values: The upper grid cell's albedo is larger when snow-covered compared to snow-free conditions in contrast to the energy balance parameters. An increasing SAF with increased albedo median differences can be expected as a larger albedo difference induces larger net shortwave radiation gains at the upper grid cell in the snow-free sample. This is, however, not obtained in MAM (see Fig. 4a), which indicates that albedo median

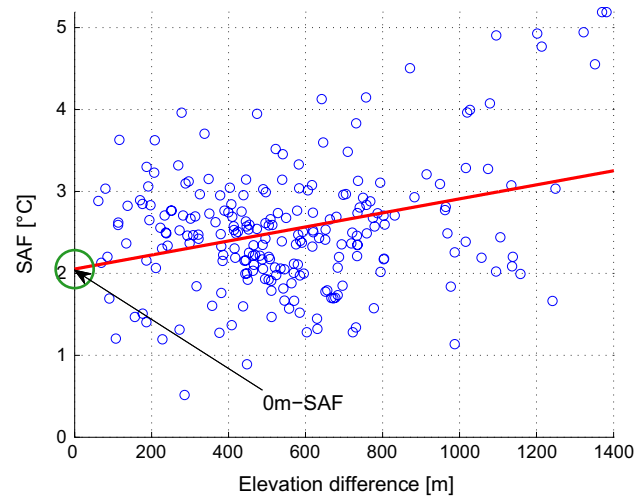


Fig. 5 Relationship between the diagnosed SAF and the elevation differences in ETHZ-CLM for MAM. Each *circle* represents one grid cell pair's SAF as a function of the respective elevation difference. The correlation is indicated using a linear regression (*red line*) over all data points. The regressed SAF for an elevation difference of 0 m yields the 0m-SAF

differences are not the controlling factor for the SAF variability.

The net shortwave radiation median differences are positive at all grid cell pairs (x-axis in Fig. 4e). A particular illustrative grid cell pair (filled circle) indicates that the upper grid cell, when snow-free, reveals approximately 48 W m^{-2} more net solar radiation at the surface, than when snow-covered. Furthermore, a clear positive correlation between net shortwave radiation differences and the diagnosed SAF is found.

On the other hand, net longwave radiation median differences mostly reveal negative values (x-axis in Fig. 4c), possibly due to a restriction of surface temperatures not exceeding $0 \text{ }^{\circ}\text{C}$ above snow. This induces less outgoing longwave radiation and larger net longwave radiation at the surface for snow cover compared to snow-free conditions. A rather unexpected result is the strong negative correlation between net longwave radiation median differences and SAF intensity. A possible reason for this negative correlation is the small range of median differences compared to the overall SAF magnitude and the range of median shortwave radiation differences. This indicates a spurious correlation via a further controlling parameter such as cloud cover. Indeed, a study by Cess et al. (1991) who investigated the SAF in different GCMs revealed that the SAF induces different climate responses. Apart from the shortwave radiation effect due to a reduction in surface albedo, there are also indirect effects via cloud cover or longwave radiation feedbacks. Clouds cause larger incident longwave radiation and smaller incident shortwave radiation.

Comparing the net shortwave and longwave radiation median differences to each other reveals a negative correlation (not shown) between these variables. This further indicates the existence of interactive effects produced by cloud cover differences between the *HS* and *NS* sample. Another cause for the unexpected sign of the correlation between SAF and net longwave radiation differences may be the sampling of specific weather situations for the quantification of median differences.

Both latent and sensible heat flux reveal positive median differences (x-axes in Fig. 4b, d), which indicates an energy surplus on snow-free days compared to snow-covered conditions (compared to net shortwave radiation). However, only sensible heat flux shows a positive correlation with the SAF.

For all surface energy components addressed, median differences are largest for net shortwave radiation (followed by sensible heat flux), implying that the main reason for the energy surplus under snow-free conditions is an increased shortwave radiation budget, which is transferred to the atmosphere via an increased flux of sensible heat. Net surface shortwave radiation differences furthermore reveal a large correlation coefficient with the diagnosed SAF, which is in agreement with our expectations based on physical considerations mentioned before. Net shortwave radiation can hence be considered as the driving variable controlling the SAF.

3.1.3 Elevation difference dependence of the SAF

Our analysis reveals that the elevation difference between two neighbouring grid cells influences the magnitude of the diagnosed SAF. For MAM, Fig. 5 shows an increase

of SAF values with larger elevation differences. A possible reason for this effect are different regional-scale lapse rates in the two samples *HS* and *NS*. Such differences in prevailing lapse rates would become more important for the diagnosed SAF with increasing elevation difference between the grid cells. Indeed, a more detailed analysis reveals a larger large-scale lapse rate for the *HS* sample for most seasons (not shown), which induces larger SAF values with increasing elevation differences. However, this influence is too weak to entirely explain the elevation difference dependence of the SAF. To provide more insight into this issue, the role of net shortwave radiation, i.e., the key driving variable of the SAF as identified above (see Sect. 3.1.2) is analysed in more detail. Namely, the median difference of net shortwave radiation for the *HS* and the *NS* samples in MAM is related to the elevation difference. A clear positive relation is found (Fig. 6a), and we conclude that net shortwave radiation is likely responsible for the elevation difference dependence of the SAF.

The specific cause is the larger incident solar radiation at higher elevations, especially for regions higher than about 2000 m (see Fig. 6b). The larger the elevation difference, the larger are the differences in incoming solar radiation between the upper and lower grid cell. Note that the larger spread of incident solar radiation at elevations below about 1000 m that is apparent in Fig. 6b results from the fact that grid cells South of the Alps generally show larger mean incoming solar radiation than grid cells to the North.

A systematically larger albedo at high reaches for snow-free conditions could mitigate the effect of a larger

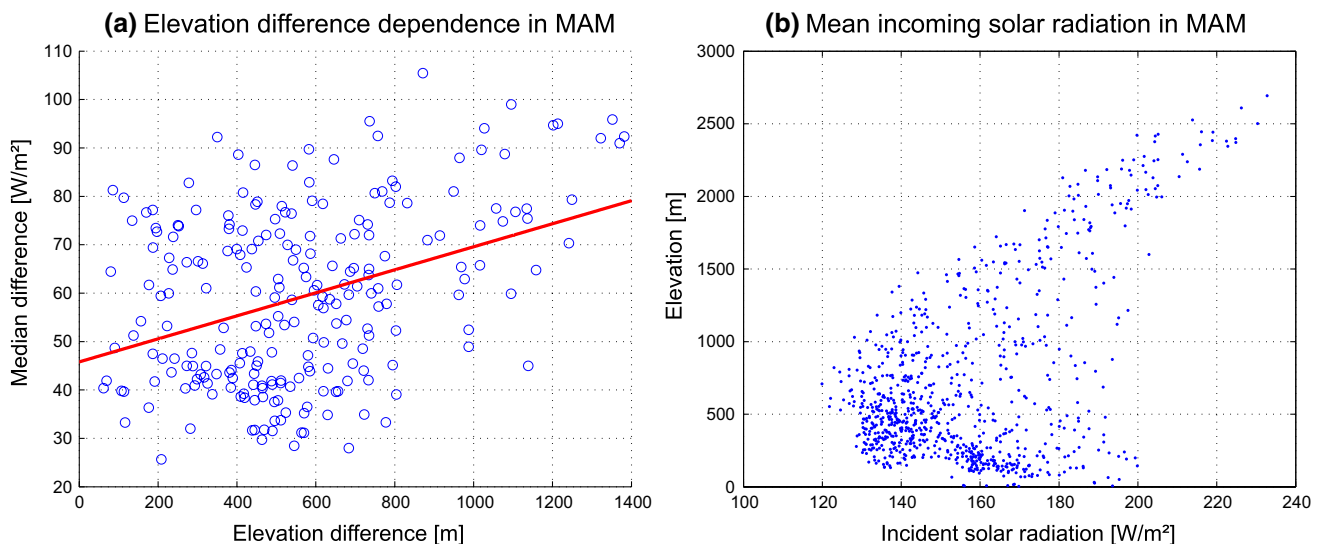


Fig. 6 Physical drivers of the SAF for ETHZ-CLM in MAM: **a** Relationship between differences in elevation and surface net shortwave radiation median differences. The linear regression (red line) is calcu-

lated over all data points (blue circles). **b** Mean incoming shortwave radiation of each grid cell over 1961–2000 for different elevations

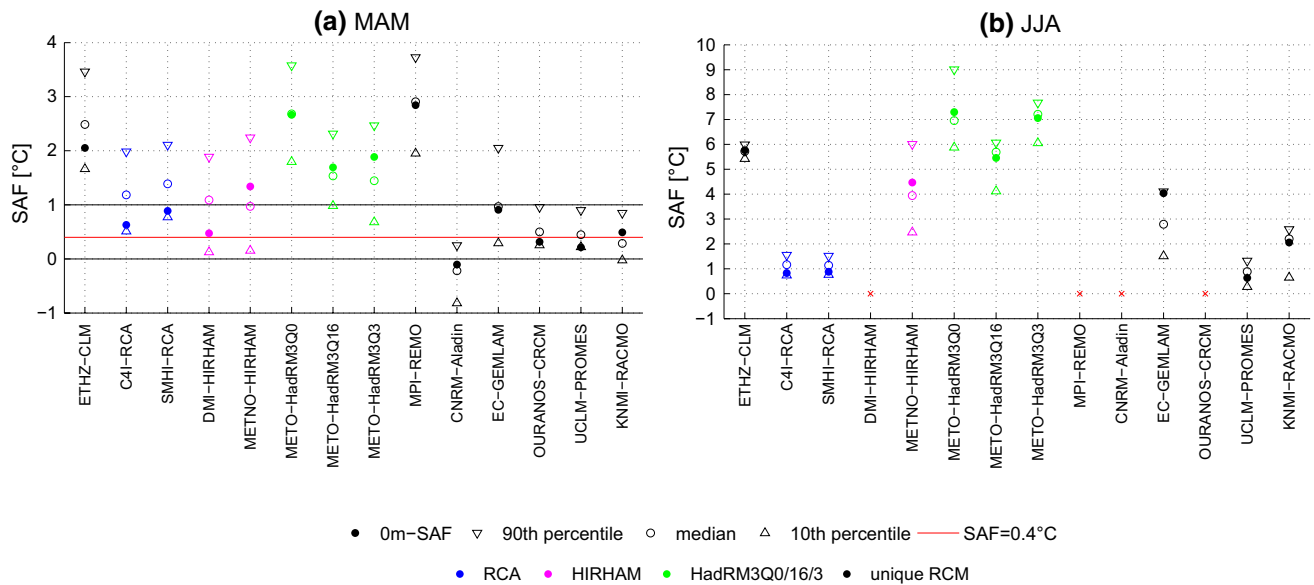


Fig. 7 SAF in 14 ERA40-driven RCMs of the ENSEMBLES project for the period 1961–2000 and for **a** MAM and **b** JJA. Shown are the diagnosed 0m-SAF, as well as the SAF-distribution in terms of the 10th and 90th percentile and the median. Note the *black lines* in **(a)** indicating an acceptable range of SAF values (based on the MAM

SAF of 0.4 °C derived by S2012) and the different scales on the vertical axis in **(b)**. The ‘x’-symbol indicates that the SAF could not be diagnosed in the particular model. The *colour coding* of the *markers* indicates the RCM applied (*coloured markers* for the same RCM/ RCM family, *black markers* for unique RCMs)

incoming solar radiation at higher elevations. Even though this effect is apparent, the albedo differences between the upper and lower grid cells are too small to mitigate entirely the higher incident solar radiation at higher elevations (not shown).

The elevation difference dependence of the diagnosed SAF suggests a normalization of the SAF over elevation differences by extrapolating the linear regression line to 0 m (=0m-SAF, see green circle in Fig. 5). This is essential in order to compare different seasons and models. The 0m-SAF is used as primary estimate in the remainder of this study, but results are usually complemented by those obtained for the PDF-based SAF estimates.

3.2 Quantification in the multi-model ensemble

Figure 7 illustrates the diagnosed spring and summer SAFs in all 14 ERA40-driven RCMs of Table 1. Typically SAF values are positive, which indicates higher temperatures for snow-free conditions compared to snow coverage. In general, larger SAFs are found for JJA (note the different y-axis scales) which presumably derives from the higher incident solar radiation in summer (e.g., Cess et al. 1991; Barry and Chorley 2010). C4I-RCA, SMHI-RCA and UCLM-PROMES show a similar SAF for both seasons. Several models have insufficient days in the *HS* sample in JJA, and consequently do not allow diagnosis of a SAF in this particular season.

The diagnosed SAF differs strongly between the analysed RCMs; ETHZ-CLM, METO-HadRM3Q0 and MPI-REMO show consistently the largest SAF. These inter-model differences may result from differences in 2m temperature diagnosis and physical parameterizations. Qu and Hall (2007) suggest that SAF differences could also result from differences in surface albedo parameterization and the explicit treatment of vegetation canopy. Models with a higher albedo over snow in general reveal a strong albedo difference between snow-covered and snow-free conditions.

3.3 Discussion

The SAF quantification for the models of the ENSEMBLES project reveals mostly larger values than derived by S2012 for MAM (0.4 °C). For instance, the diagnosed SAF in ETHZ-CLM for MAM strongly exceeds that reference value (0m-SAF of 2.05 °C). This may derive from a negative temperature bias over snow and ice as reported by Buzzi (2008). Other models may suffer from this bias characteristic as well. In these particular cases, the term SAF is misleading, since the diagnosed SAF might primarily result from a particular bias structure of the model rather than from a physically consistent representation of the SAF. The overestimation of the diagnosed SAF at higher reaches may be strongly connected to the cold bias found at high elevations in several RCMs (e.g., Kotlarski

et al. 2015). In principle, also scale issues might be responsible for the SAF overestimation by many RCMs. While S2012 derived their springtime SAF estimate from station pairs, we here transfer their approach to the RCM grid cell-scale and compare neighbouring grid cells that represent mean conditions for cells of about $25 \times 25 \text{ km}^2$ size. Scale effects, for instance, could be related to local temperature inversions affecting temperature differences for individual station pairs but that are not represented by the coarsely resolved RCM output. However, as the employed snow parameterization schemes are based on independent column approaches (partly accounting for subgrid variability, though; see Sect. 2.2) and as the SAF validation is not carried out on a grid cell-by grid cell but on an Alpine-wide regional scale, we believe that scale issues do not play a deciding role. In contrast, representativeness issues might be able to partly explain the apparent SAF overestimation in the RCMs. Topographic shading effects with their influence on both the longwave and the shortwave surface radiation balance are not accounted for in the models but might partly influence (here: lower) the SAF estimates derived by S2012 based on station observations.

One model (CNRM-Aladin) reveals mostly negative SAF values in MAM (for both regional SAF and 0m-SAF). This indicates that the temperature in this model is typically higher if the grid cell is snow-covered, compared to snow-free conditions at that particular time of the year. The reason for this behaviour has not been further investigated.

On a regional scale and for a given model and a given season, a considerable spread of the diagnosed SAF is apparent. This spread can partly be explained by the elevation difference between the upper and the lower grid cell of a given grid cell pair and the underlying elevation dependency of the shortwave radiation budget. However, elevation differences cannot fully explain the SAF spread as there is, for instance, a considerable scatter of SAF values within each individual elevation difference class (not shown). Furthermore, elevation differences cannot fully explain the SAF spread obtained when computing the SAF of a single local maximum grid cell separately based on its eight lower-elevation neighbours (not shown).

In the multi-model ensemble, C4I-RCA, SMHI-RCA, DMI-HIRHAM, EC-GEMLAM, OURANOS-CRCM, UCLM-PROMES and KNMI-RACMO reveal a rather realistic SAF between 0 and $1 \text{ }^\circ\text{C}$ in MAM. The quantification of the contribution of the SAF to twenty first century temperature changes in the European Alps in the following section will therefore be primarily based on these models.

4 SAF in climate scenarios

The following section presents estimates of the contribution of the diagnosed SAF to spring and summer Alpine temperature changes in the twenty first century (ΔT_{SAF}) using the method described in Sect. 2.5. For this purpose, the GCM-driven RCMs listed in Table 1 are considered. As a consequence of the results in Sect. 3.2, the interpretation distinguishes between models revealing a realistic SAF (compared to S2012; further referred to as *SAF models*). *Other models* show an unrealistically high or low SAF. Scenario experiments contributing to the *SAF models* suite are: DMI-ARPEGE, KNMI-ECHAM5, SMHI-BCM/ECHAM5/HadCM3Q3. The remaining models listed in Table 1 contribute to the *other models* suite. *SAF model* contributions can be assumed to mostly derive from the SAF, whereas *other models'* contributions may for instance derive from snow cover-dependent temperature biases and their interpretation is more complex.

4.1 Contribution to future temperature changes

The contribution of the SAF to future temperature changes is calculated using the diagnosed 0m-SAF. In addition the contributions assuming the median, 10th and 90th percentile SAFs are computed. The latter illustrate the range of possible SAF contributions given uncertainties of the SAF quantification. Figure 8a–d illustrates ΔT_{SAF} in every RCM scenario averaged over the entire analysis domain. Contributions are typically larger in JJA (up to $1.3 \text{ }^\circ\text{C}$) compared to MAM (up to $0.28 \text{ }^\circ\text{C}$).

ΔT_{SAF} reveals large inter-model differences owing to (a) differences in the diagnosed SAF values (see Sect. 3.2) and (b) different changes of snow cover due to the overall warming magnitude (cf. Steger et al. 2013). The three SMHI simulations (driven by different GCMs but applying the same RCM) show similar SAF contributions, as changes in snow cover are similar in all simulations, and as the analysis uses the same seasonal SAF values quantified in Sect. 3.2 from the ERA40-driven simulation. DMI-ARPEGE and KNMI-ECHAM5 reveal the smallest contribution for almost every season, typically smaller than $0.1 \text{ }^\circ\text{C}$. The two model samples (*SAF models* and *other models*) show distinctly different ΔT_{SAF} values in MAM and JJA. The larger contribution in *other models* derives from a larger diagnosed SAF in these seasons. In addition, Fig. 8b (black squares) illustrates the SAF contribution in MAM using the SAF as diagnosed from observational data by S2012 ($0.4 \text{ }^\circ\text{C}$) for every model according to Eq. 2. Contributions ranging from 0 to $0.1 \text{ }^\circ\text{C}$ are obtained. A similar ΔT_{SAF} of DMI-ARPEGE and KNMI-ECHAM5 when assuming the $0.4 \text{ }^\circ\text{C}$ -SAF compared to the model-specific

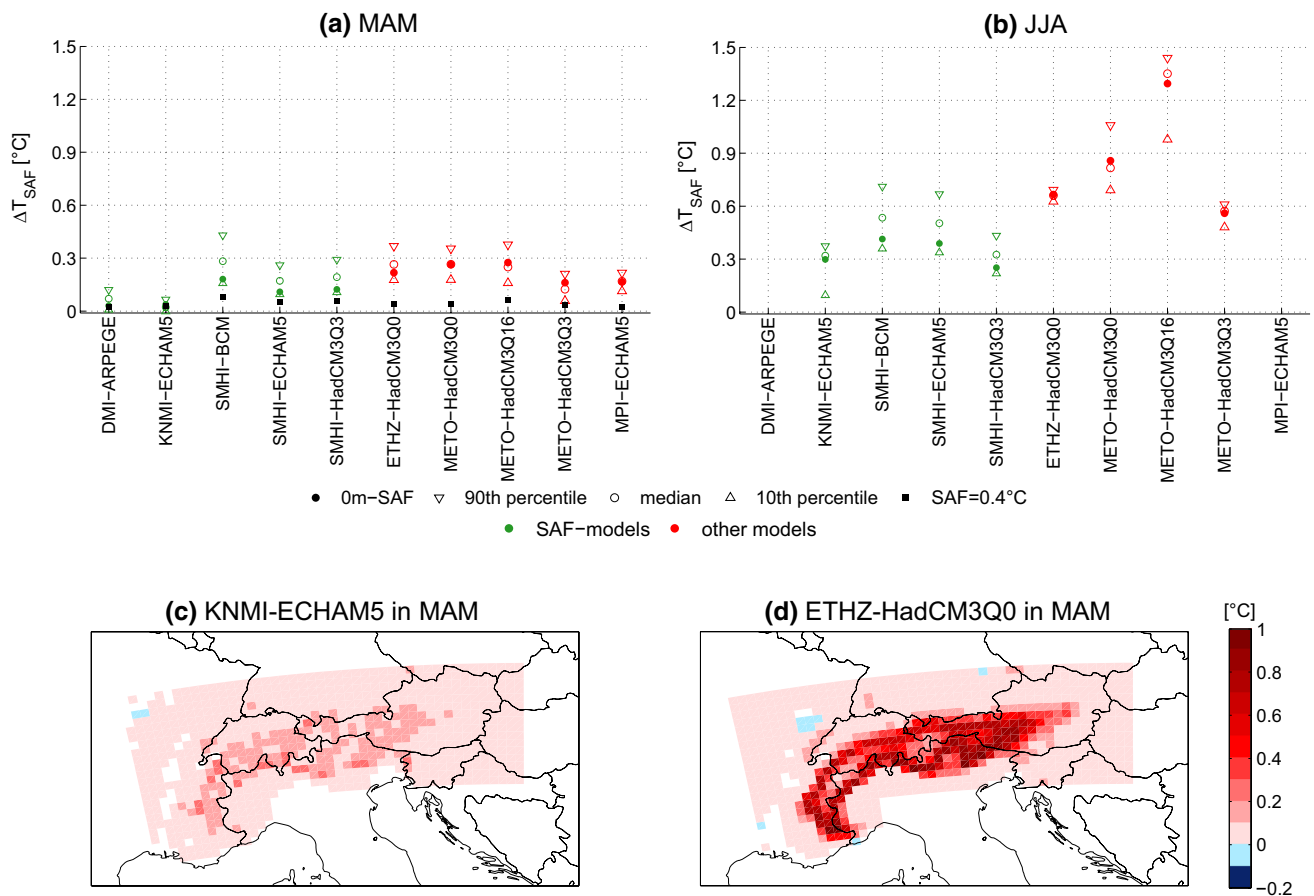


Fig. 8 Regional contribution of the SAF to future mean seasonal temperature changes (ΔT_{SAF}) in **a** MAM and **b** JJA by *SAF models* (green) and *other models* (red) averaged over the whole analysis domain. In JJA, no contribution can be quantified in DMI-ARPEGE and MPI-ECHAM5 because no SAF was diagnosed in the corresponding ERA40-driven simulation. **c**, **d** Illustrate the spatial dis-

tribution of ΔT_{SAF} in MAM of one *SAF model* (KNMI-ECHAM5) and one *other model* (ETHZ-HadCM3Q0). White grid cells in the analysis domain do not show any snow day change and consequently no ΔT_{SAF} is available. These grid cells have no contribution to the domain mean numbers

SAF derives from a diagnosed SAF close to 0.4 °C. Yet, all *other models* reveal a larger contribution when using the (larger) model-specific SAF.

The inter-model differences mainly derive from differences in the SAF and not from strongly differing ΔSD , as can be seen from the small spread of the MAM SAF contribution assuming the 0.4 °C SAF. Figure 8e–f illustrates the spatial variability of ΔT_{SAF} for MAM over the analysis domain, assuming the 0m-SAF. For illustration purposes only one *SAF model*, which reveals a similar MAM SAF as diagnosed by S2012 (KNMI-ECHAM5) and one *other model* (ETHZ-HadCM3Q0) are displayed. Larger ΔT_{SAF} values are obtained for ETHZ-HadCM3Q0 as a result of a larger diagnosed SAF in MAM. For both models the spatial distribution of ΔT_{SAF} is strongly connected to the surface orography (cf. Fig. 1) and typically increases with elevation. However, the maximum contribution is not obtained at peak elevation, but at somewhat lower elevations.

The estimated MAM SAF contributions at specific grid cells can be much larger than the domain-mean contributions (see Fig. 8c and d). This can be explained by the fact that most of the analysis domain consists of grid cells located at lower elevations, which are not sensitive to the SAF and show a small or even negative SAF contribution. Negative values occur when grid cells show a more frequent snow cover in the future (2070–2099) compared to the reference period (1971–2000). This is only the case for individual low-elevation grid cells with very few snow-covered days in the control period and can be attributed to internal climate variability. The obviously elevation-dependent ΔT_{SAF} suggests an analysis of the SAF contribution for distinct elevation bands in order to gain a better insight into the governing processes and into SAF contributions at sub-regional scales.

For this purpose, Fig. 9 illustrates the absolute and percentage ΔT_{SAF} at different elevations for the *SAF*

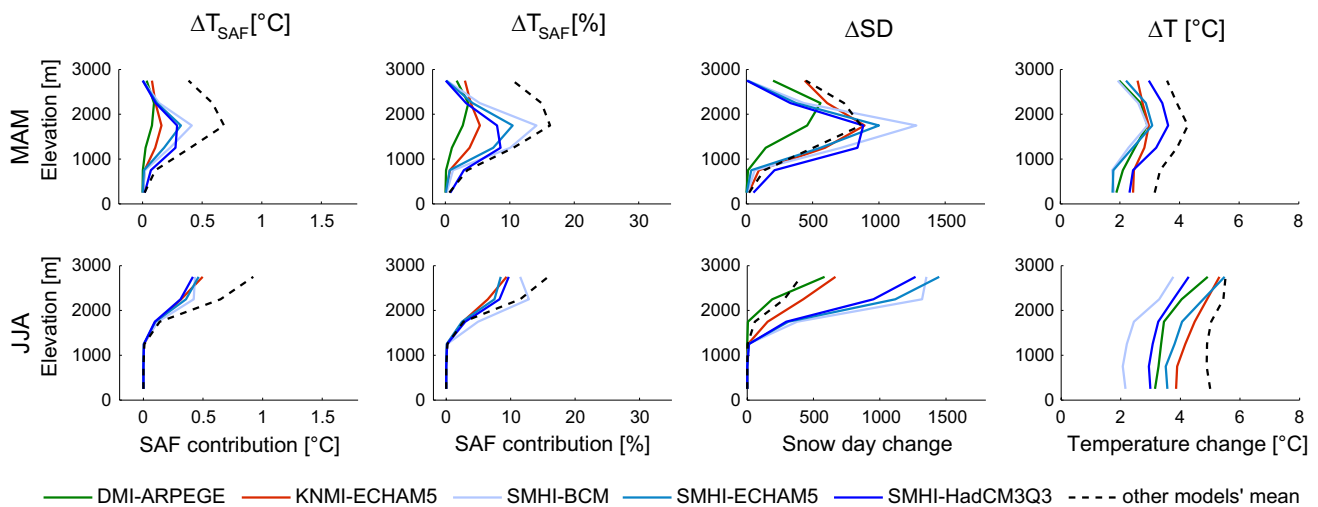


Fig. 9 SAF contribution to future temperature changes (ΔT_{SAF}), snow day changes (ΔSD ; loss of snow days per 30-year period) and temperature changes (ΔT) in 500 m elevation classes for *SAF models*

and a mean over *other models* in MAM (*upper row*) and JJA (*lower row*) using the 0m-SAF. Note that DMI-ARPEGE does not diagnose a SAF in JJA and therefore no ΔT_{SAF} can be computed

models. *Other models'* contributions are indicated as a multi-model mean (mean over all *other models*: ETHZ-HadCM3Q0, METO-HadCM3Q0/Q16/Q3 and MPI-ECHAM5). Additionally the change of snow days (ΔSD ; absolute loss of snow days for an entire 30-year period) and the total temperature change (ΔT) are shown to better understand the elevation-dependent behaviour of ΔT_{SAF} . Maximum values are obtained at similar elevations for all parameters in all models and seasons. A shift to higher elevations from MAM to JJA qualitatively agrees with the shift of the zero-degree line (Ceppi et al. 2012). Elevations where the maximum SAF contribution is reached are located between 1500 and 2000 m in MAM and above 2000 m in JJA. At lower reaches the SAF contribution vanishes completely since no ΔSD is apparent. All *SAF models* reveal a maximum absolute contribution between 0 and 0.5 °C, indicating a distinct influence of the SAF on the temperature change at medium and high elevations. This is also visible in the percentage contribution ranging from 0 to 14.1 % in MAM and to 12.8 % in JJA. DMI-ARPEGE shows consistently the lowest contribution (maximal 0.1 °C in MAM), whereas all SMHI experiments show similarly high contributions (maximal 0.29 to 0.41 °C in MAM).

ΔSD is elevation-dependent and ranges from no change at low elevations (below about 500 m in MAM and 1300 m in JJA) to reductions of 1000 days and more at medium elevations around 1800 m in MAM and high elevations above 2000 m in JJA. The elevation of maximum ΔT_{SAF} typically coincides with the elevation of maximum ΔSD , which

is in agreement with our expectations based on Eq. 2. In both MAM and JJA also the maximum overall temperature change ΔT occurs at these elevations, pointing to a general amplification of the warming signal in regions of strong snow cover reduction by the SAF in these seasons. Note that very high elevations above 3000 m are not covered by the RCMs applied in the present work. Here, an increase of the number of snows days and, hence, a negative ΔT_{SAF} might in principle be possible due to low temperature levels and slightly increasing mid-winter snowfall sums in some models (see, e.g., Steger et al. 2013).

Comparing *SAF models* and *other models* in the elevation-dependent analysis reveals systematic differences. ΔSD is typically similar in both model classes. The absolute ΔT_{SAF} is larger in both MAM and JJA in the *other model* mean, which derives from the larger diagnosed SAF in these models. The respective percentage ΔT_{SAF} signal is damped because the *other model* mean shows the highest ΔT . ΔT is similar for models driven by the same GCM, which is in agreement with earlier studies (e.g., Steger et al. 2013; Räisänen and Eklund 2012). However differences are still apparent, especially between *SAF models* and *other models* driven by the same GCM (i.e., SMHI-HadCM3Q3 and METO-HadCM3Q3, not shown), which reveals the non-negligible influence of the RCM on temperature changes, and additionally might also highlight an overestimation of future temperature changes in regions of strong snow cover decreases by *other models* as a consequence of snow cover-dependent temperature biases.

4.2 Discussion

The analysis presented above suggests a distinct contribution of the SAF to future Alpine temperature changes and reveals spatial variabilities of this contribution. As such, ΔT_{SAF} values averaged over the whole domain only provide a limited picture as they do not show the actual temperature changes originating from the grid cell-scale SAF process. However, the domain-mean values are still relevant as they denote the mean additional warming for the whole analysis domain due to the diagnosed SAF. ΔT_{SAF} is strongly coupled to ΔSD . ΔT_{SAF} in *SAF models* shows a distinct estimated SAF contribution to future temperature changes in MAM of approx. 0.26 °C or 8 % (mean of all *SAF models*) of the overall temperature change at elevations with maximum contributions. Interestingly, the derived percentage contribution is similar to the one diagnosed by S2012 for the period 1961–2011 using observational data. In JJA the maximum contribution of the *SAF model* mean amounts to 0.45 °C or 10 % of the overall temperature change. Significantly larger values in the *other model* mean, as a result of a SAF overestimation, point to non-stationary temperature biases in these models and could to some extent be used as a process-dependent temperature bias correction. Note that removing the SAF contribution (ΔT_{SAF}) would not remove the elevation dependency of ΔT itself (visible in the right panels of Fig. 9). Therefore the SAF alone cannot explain the elevation dependence of future temperature changes and further elevation-dependent forcings are likely to be involved (see Kotlarski et al. 2012, for further details).

5 Conclusions and Outlook

The present study evaluates the capability of the ENSEMBLES RCMs to represent the Alpine SAF and assesses the contribution of this feedback to future temperature changes in spring and summer. The SAF is diagnosed applying the method introduced by S2012. Regarding the objectives listed in Sect. 1, the study finds the following:

1. RCMs of the ENSEMBLES project are, in principle, able to capture the SAF. Resulting SAF values are typically positive, i.e., snow cover reductions induce an increase of 2m temperatures. However, the range of diagnosed SAF values is large. A SAF close to the observation-based value is diagnosed in several models, but the SAF is considerably overestimated in others.
2. Net shortwave radiation has the largest influence of all components of the energy balance on the diagnosed SAF and can partly explain the diagnosed SAF differences.

3. The widespread SAF overestimation may originate from model deficiencies in reproducing 2m temperatures above snow (Buzzi 2008). Large SAF values may therefore be connected to observed negative temperature biases at high elevations (Kotlarski et al. 2015).
4. The estimated contribution of the SAF to twenty first century temperature changes is calculated based on snow day changes, which are strongly dependent on elevation (Ceppi et al. 2012). The most sensitive elevations vary with season. In MAM, maximum SAF contributions are located between 1500 and 2000 m and in JJA at elevations above 2000 m. Until the end of the twenty first century, a temperature change between 0 and 0.5 °C or between 0 and 14 % of the total temperature change at elevations of maximum contribution is estimated to originate from the SAF. In MAM, the maximum contribution of the multi-model mean amounts to 0.26 °C or 8 % of the overall temperature change.

The models overestimating the SAF are likely subject to snow cover-dependent temperature biases and—as a consequence of future snow cover reductions—to non-stationary model biases. In particular, assuming a constant model bias in the common delta-change approach may yield a too large future Alpine warming signal in these models, and may distort our perception of twenty first century temperature changes.

To reveal uncertainties in the SAF quantification of the entire RCM ensemble (e.g., SWE threshold or elevation dependence), a detailed and process-based validation of the SAF, as presented for ETHZ-CLM in the present work, would be necessary for each individual RCM. Such an analysis should in particular address shortcomings in the respective 2m temperature diagnostics and should include a separate analysis of temperature biases under snow-covered and snow-free conditions. Since net longwave radiation at the surface reveals a large influence on the SAF and is mainly controlled by cloud cover, additional analyses on the correlation between specific weather situations and SAF intensity may lead to a better understanding of the large spread of SAF values and the negative correlation between SAF and net longwave radiation at the surface. The present work did not cover these aspects in detail and for the entire RCM ensemble employed here. As a consequence, the estimated SAF contribution to future temperature changes has to be put into perspective since it is contingent on a proper representation of the Alpine SAF in the underlying RCMs. Although models showing strongly biased SAF values were removed from the climate scenario analysis, a certain contribution of model-specific SAF misrepresentations cannot be ruled out. These remaining issues, for instance, concern model shortcomings in the representation of a stable

boundary layer and of 2m temperature diagnostics (e.g., Buzzi 2008) but can also include deficient representations of snow albedo (e.g., Pirrazini 2009) with corresponding effects on the surface radiation budget.

In the future, the availability of convection-resolving climate scenarios at the kilometre-scale (e.g., Ban et al. 2014, 2015; Kendon et al. 2014) can be expected to provide further insight into the importance of the SAF for future temperature changes in the European Alps. In particular, this is true for high elevations above 3000 m that are not yet covered by the 25 km-resolution RCMs of the ENSEMBLES project. As an intermediate step, the 12 km grid-spacing experiments of the EURO-CORDEX initiative (Jacob et al. 2014; Kotlarski et al. 2014) should be exploited and results could be compared to those of the present work. EURO-CORDEX provides a considerably larger model ensemble and explicitly considers several emission scenarios. However, on regional scales the performance of EURO-CORDEX is comparable to the performance of the ENSEMBLES runs (e.g., Kotlarski et al. 2014) and the ENSEMBLES database used in the present work is far from being outdated.

Acknowledgments The ENSEMBLES data used in this work was funded by the EU FP6 Integrated Project ENSEMBLES (Contract No. 505539) whose support is gratefully acknowledged. This research was partly funded by the Swiss National Science Foundation through the SNSF Sinergia project CRSII2_136279 “The Evolution of Mountain Permafrost in Switzerland” (TEMPS).

References

- Appenzeller C, Begert M, Zenklusen E, Scherrer SC (2008) Monitoring climate at Jungfrauoch in the high Swiss Alpine region. *Sci Total Environ* 391(2–3):262–268. doi:10.1016/j.scitotenv.2007.10.005
- Armstrong RL, Brun E (2008) Snow and climate: physical processes, surface energy exchange and modeling. Cambridge University Press, Cambridge
- Ban N, Schmidli J, Schär C (2014) Evaluation of the convection-resolving regional climate modeling approach in decade-long simulations. *J Geophys Res Atmos* 119(13):7889–7907. doi:10.1002/2014JD021478
- Ban N, Schmidli J, Schär C (2015) Heavy precipitation in a changing climate: does short-term summer precipitation increase faster? *Geophys Res Lett* 42(4):1165–1172. doi:10.1002/2014GL062588
- Barry R, Gan TY (2011) The global cryosphere: past, present and future. Cambridge University Press, Cambridge
- Barry RG, Chorley RJ (2010) Atmosphere, weather and climate, 9th edn. Routledge, London and New York
- Boone A, Etchevers P (2001) An intercomparison of three snow schemes of varying complexity coupled to the same land surface model: local-scale evaluation at an Alpine site. *J Hydrometeorol* 2(4):374–394. doi:10.1175/1525-7541(2001)002<0374:AIOTSS>2.0.CO;2
- Bradley RS, Keimig FT, Diaz HF (2004) Projected temperature changes along the American cordillera and the planned GCOS network. *Geophys Res Lett* 31:L16210. doi:10.1029/2004GL020229
- Buzzi M (2008) Challenges in operational numerical weather prediction at high resolution in complex terrain. Ph.D. thesis, ETH Zurich
- Ceppi P, Scherrer SC, Fischer AM, Appenzeller C (2012) Revisiting Swiss temperature trends 1959–2008. *Int J Climatol* 32(2):203–213. doi:10.1002/joc.2260
- Cess RD, Potter GL, Zhang M-H, Blanchet J-P, Chaila S, Colman R, Dazlich DA, del Genio AD, Dymnikov V, Galin V, Jerrett D, Keup E, Lacis AA, Le Treut H, Liang X-Z, Mahfouf J-F, McAvaney BJ, Meleshko VP, Mitchell JFB, Morcrette J-J, Norris PM, Randall DA, Rikus L, Roeckner E, Royer J-F, Schlese U, Sheinin DA, Slingo JM, Sokolov AP, Taylor KE, Washington WM, T WR, Yagai I (1991) Interpretation of snow-climate feedback as produced by 17 general circulation models. *Science* 253(5022):888–892. doi:10.1126/science.253.5022.888
- Collins M, Knutti R, Arblaster J, Dufresne J-L, Fichefet T, Friedlingstein P, Gao X, Gutowski WJ, Johns T, Krinner G, Shongwe M, Tebaldi C, Weaver AJ, Wehner M (2013) Long-term climate change: projections, commitments and irreversibility. In: Stocker TF, Qin D, Plattner G-K, Tignor M, Allen SK, Boschung J, Nauels A, Xia Y, Bex V, Midgley PM (eds) *Climate Change 2013: The Physical Science Basis. Contribution of Working Group I to the Fifth Assessment Report of the Intergovernmental Panel on Climate Change*, Cambridge University Press, Cambridge, United Kingdom and New York, NY, USA
- Colman R (2003) A comparison of climate feedbacks in general circulation models. *Clim Dyn* 20(7–8):865–873. doi:10.1007/s00382-003-0310-z
- Doms G, Frstner J, Heise E, Herzog H-J, Mironov D, Raschendorfer M, Reinhardt T, Ritter B, Schrodin R, Schulz J-P, Vogel G (eds) (2011) A description of the nonhydrostatic regional COSMO Model. Part II: physical parameterization, COSMO Consortium for small-scale modelling. www.cosmo-model.org
- Fernandes R, Zhao H, Wang X, Key J, Qu X, Hall A (2009) Controls on Northern Hemisphere snow albedo feedback quantified using satellite Earth observations. *Geophys Res Lett* 36:L21702. doi:10.1029/2009GL040057
- Giorgi F, Hurrell JW, Marinucci MR, Beniston M (1997) Elevation dependency of the surface climate change signal: a model study. *J Clim* 10(2):288–296. doi:10.1175/1520-0442(1997)010<0288:EDO TSC>2.0.CO;2
- Graversen RG, Langen PL, Mauritsen T (2014) Polar amplification in CCSM4: Contributions from the lapse rate and surface albedo feedbacks. *J Clim* 27(12):4433–4450. doi:10.1175/JCLI-D-13-00551.1
- Hall A (2004) The role of surface albedo feedback in climate. *J Clim* 17(7):1550–1568. doi:10.1175/1520-0442(2004)017<1550:TRO SAF>2.0.CO;2
- Jacob D, Petersen J, Eggert B, Alias A, Christensen OB, Bouwer LM, Braun A, Colette A, Déqué M, Georgievski G, Georgopoulou E, Gobiet A, Menut L, Nikulin G, Haensler A, Hempelmann N, Jones C, Keuler K, Kovats S, Kröner N, Kotlarski S, Kriegsmann A, Martin E, van Meijgaard E, Moseley C, Pfeifer S, Preuschmann S, Radermacher C, Radtke K, Rechied D, Rounsevell M, Samuelsson P, Somot S, Soussana J-F, Teichmann C, Valentini R, Vautard R, Weber B, Yiou P (2014) EURO-CORDEX: new high-resolution climate change projections for European impact research. *Reg Environ Change* 14(2):563–578. doi:10.1007/s10113-013-0499-2
- Kendon EJ, Roberts NM, Fowler HJ, Roberts MJ, Chan SC, Senior CA (2014) Heavier summer downpours with climate change revealed by weather forecast resolution model. *Nature Clim Change* 4:570–576. doi:10.1038/nclimate2258

- Kotlarski S, Bosshard T, Lüthi D, Pall P, Schär C (2012) Elevation gradients of European climate change in the regional climate model COSMO-CLM. *Clim Change* 112(2):189–215. doi:[10.1007/s10584-011-0195-5](https://doi.org/10.1007/s10584-011-0195-5)
- Kotlarski S, Keuler K, Christensen OB, Colette A, Déqué M, Gobiet A, Goergen K, Jacob D, Lüthi D, van Meijgaard E, Nikulin G, Schär C, Teichmann C, Vautard R, Warrach-Sagi K, Wulfmeyer V (2014) Regional climate modelling on European scales: a joint standard evaluation of the EURO-CORDEX RCM ensemble. *Geosci Model Dev* 7(1):1297–1333. doi:[10.5194/gmd-7-1297-2014](https://doi.org/10.5194/gmd-7-1297-2014)
- Kotlarski S, Lüthi D, Schär C (2015) The elevation dependency of 21st century European climate change: an RCM ensemble perspective. *Int J Climatol*. doi:[10.1002/joc.4254](https://doi.org/10.1002/joc.4254)
- Laternser M, Schneebeli M (2003) Long-term snow climate trends of the Swiss Alps (1931–99). *Int J Climatol* 23(7):733–750. doi:[10.1002/joc.912](https://doi.org/10.1002/joc.912)
- Lawrence DM, Slater AG (2010) The contribution of snow condition trends to future ground climate. *Clim Dyn* 34(7–8):969–981. doi:[10.1007/s00382-009-0537-4](https://doi.org/10.1007/s00382-009-0537-4)
- Lawrence DM, Oleson KW, Flanner MG, Thornton PE, Swenson SC, Lawrence PJ, Zeng X, Yang Z-L, Levis S, Sakaguchi K, Bonan GB, Slater AG (2011) Parameterization improvements and functional and structural advances in version 4 of the community land model. *J Adv Model Earth Syst* 3:M03001. doi:[10.1029/2011MS000045](https://doi.org/10.1029/2011MS000045)
- van der Linden P, Mitchell JFB (eds) (2009) ENSEMBLES: climate change and its impacts: summary of research and results from the ENSEMBLES project, Met Office Hadley Centre, FitzRoy Road, Exeter EX1 3PB, UK
- Marty C (2008) Regime shift of snow days in Switzerland. *Geophys Res Lett* 35:L12501. doi:[10.1029/2008GL033998](https://doi.org/10.1029/2008GL033998)
- Nakićenović N, Swart R (eds) (2000) Emissions scenarios. A special report of Working Group III of the Intergovernmental Panel on Climate Change, Cambridge University Press, Cambridge, United Kingdom and New York, NY, USA
- Ohmura A (2001) Physical basis for the temperature-based melt-index method. *J Appl Meteorol* 40(4):753–761. doi:[10.1175/1520-0450\(2001\)040<0753:PBFTTB>2.0.CO;2](https://doi.org/10.1175/1520-0450(2001)040<0753:PBFTTB>2.0.CO;2)
- Peixoto JP, Oort AH (1992) *Physics of climate*. American Institute of Physics, New York
- Pepin N, Bradley RS, Diaz HF, Baraer M, Caceres EB, Forsythe N, Fowler H, Greenwood G, Hashmi MZ, Liu XD, Miller JR, Ning L, Ohmura A, Palazzi E, Rangwala I, Schöner W, Severskiy I, Shahgedanova M, Wang MB, Williamson SN, Yang DQ (2015) Elevation-dependent warming in mountain regions of the world. *Nature Clim Change* 5(5):424–430. doi:[10.1038/nclimate2563](https://doi.org/10.1038/nclimate2563)
- Pepin NC, Lundquist JD (2008) Temperature trends at high elevations: patterns across the globe. *Geophys Res Lett* 35:L14701. doi:[10.1029/2008GL034026](https://doi.org/10.1029/2008GL034026)
- Pirazzini R (2009) Challenges in snow and ice albedo parameterizations. *Geophysica* 45(1–2):41–62
- Qu X, Hall A (2007) What controls the strength of snow-albedo feedback? *J Climate* 20(15):3971–3981. doi:[10.1175/JCLI4186.1](https://doi.org/10.1175/JCLI4186.1)
- Räisänen J, Eklund J (2012) 21st century changes in snow climate in Northern Europe: a high-resolution view from ENSEMBLES regional climate models. *Clim Dyn* 38(11–12):2575–2591. doi:[10.1007/s00382-011-1076-3](https://doi.org/10.1007/s00382-011-1076-3)
- Rockel B, Will A, Hense A (2008) The regional climate model COSMO-CLM (CCLM). *Meteorol Z* 17(4):347–348. doi:[10.1127/0941-2948/2008/0309](https://doi.org/10.1127/0941-2948/2008/0309)
- Scherrer SC, Appenzeller C, Laternser M (2004) Trends in Swiss Alpine snow days: the role of local- and large-scale climate variability. *Geophys Res Lett* 31:L13215. doi:[10.1029/2004GL020255](https://doi.org/10.1029/2004GL020255)
- Scherrer SC, Ceppi P, Croci-Maspoli M, Appenzeller C (2012) Snow-albedo feedback and Swiss spring temperature trends. *Theor Appl Climatol* 110(4):509–516. doi:[10.1007/s00704-012-0712-0](https://doi.org/10.1007/s00704-012-0712-0)
- Scherrer SC, Wüthrich C, Croci-Maspoli M, Weingartner R, Appenzeller C (2013) Snow variability in the Swiss Alps 1864–2009. *Int J Clim* 33(15):3162–3173. doi:[10.1002/joc.3653](https://doi.org/10.1002/joc.3653)
- Soden BJ, Held IM (2006) An assessment of climate feedbacks in coupled ocean-atmosphere models. *J Clim* 19(14):3354–3360. doi:[10.1175/JCLI3799.1](https://doi.org/10.1175/JCLI3799.1)
- Steger C, Kotlarski S, Jonas T, Schär C (2013) Alpine snow cover in a changing climate: a regional climate model perspective. *Clim Dyn* 41(3–4):735–754. doi:[10.1007/s00382-012-1545-3](https://doi.org/10.1007/s00382-012-1545-3)
- Uppala SM, Kållberg PW, Simmons AJ, Andrae U, da Costa Bechtold V, Fiorino M, Gibson JK, Haseler J, Hernandez A, Kelly GA, Li X, Onogi K, Saarinen S, Sokka N, Allan RP, Andersson E, Arpe K, Balmaseda MA, Beljaars ACM, van de Berg L, Bidlot J, Bormann N, Caires S, Chevallier F, Dethof A, Dragosavac M, Fisher M, Fuentes M, Hagemann S, Hólm E, Hoskins BJ, Isaksen I, Janssen PAEM, Jenne R, McNally AP, Mahfouf J-F, Morcrette J-J, Rayner NA, Saunders RW, Simon P, Sterl A, Trenberth KE, Untch A, Vasiljevic D, Viterbo P, Woollen J (2005) The ERA-40 re-analysis. *Q J R Meteorol Soc* 131(612):2961–3012. doi:[10.1256/qj.04.176](https://doi.org/10.1256/qj.04.176)
- US Geological Survey (2014) Global 30 arc-second elevation (GTOPO30). <https://lta.cr.usgs.gov/GTOPO30>
- Vaughan DG, Comiso JC, Allison I, Carrasco J, Kaser G, Kwok R, Mote P, Murray T, Paul F, Ren J, Rignot E, Solomina O, Steffen K, Zhang T (2013) Observations: cryosphere. In: Stocker TF, Qin D, Plattner G-K, Tignor M, Allen SK, J B, Nauels A, Xia Y, Bex V, Midgley PM (eds) *Climate change 2013: the physical science basis. Contribution of Working Group I to the Fifth Assessment Report of the Intergovernmental Panel on Climate Change*, Cambridge University Press, Cambridge, United Kingdom and New York, NY, USA
- Winton M (2006) Surface albedo feedback estimates for the AR4 climate models. *J Clim* 19(3):359–365. doi:[10.1175/JCLI3624.1](https://doi.org/10.1175/JCLI3624.1)